PHASE TRANSITIONS

Effect of Fluctuations on the Formation of Secondary Phase Precipitates at Grain Boundaries

P. E. L'vov[a], * and V. V. Svetukhin[a, b]

[a] *Ulyanovsk State University, Ulyanovsk, 432017 Russia*
[b] *Institute of Nanotechnologies of Microelectronics, Russian Academy of Sciences, Moscow, 115487 Russia*
*e-mail: LvovPE@Sv.uven.ru
Received August 13, 2018; revised September 19, 2018

Abstract—Based on the free energy density functional method (modified Cahn–Hillard–Cook equation), the formation kinetics of secondary phases in binary alloys is considered in the presence of composition fluctuations and with inclusion of the grain boundaries influences. It is revealed that the existence of grain boundaries and the fluctuations at the initial stage of the phase transition can lead to the appearance of anomalous growth rate of the average precipitate size due to a competition of various decomposition mechanisms.

1. INTRODUCTION

Most of metal-based solid solutions have polycrystalline structures; i.e., they consist of a great number of grains with different orientations with respect to each other [1−5]. The conjugation regions of neighboring grains (grain boundaries) are defects of a crystal structure that can substantially influence the distribution of point defects and alloying components of alloys, the formation of secondary phases during the solid solution decomposition, and also the mechanical and other properties [1−5] that are important for practical applications of this type of material.

One of important problems of studying the properties of polycrystalline materials is establishing the influence of grain boundaries on the first-order phase transition related to the formation of secondary phase precipitates [1]. The main method of analyzing this type of phase transitions is the method of the free energy density functional [6−8] that also can be used for analyzing the formation of precipitates at the interfaces [9, 10] or at the grain boundaries [1]. In this type of phase transition (wetting phase transition), the process of formation or transformation is considered, as a rule, for a material layer disposed on grain boundaries [1, 14] or substrate boundary [9−13]. In this case, the wetting phase can be both liquid and solid [1, 9, 10, 14], and the wetting itself can be complete or partial [1, 9−14]. In the case of partial wetting, the surface layer can be transformed by the spinodal mechanism [10−13] or by the nucleation mechanism with the formation of individual precipitates at the corresponding interfaces [10−14]. The existence of wetting phase transitions at grain boundaries was experimentally observed for various metallic alloys [14−16].

In [17, 18], the free energy density functional method was used to develop the phenomenological model describing the influence of grain boundaries on the process of distribution of components between the grain-boundary region and the grain bulk. The simulation carried out in [17, 18] showed that various types of distribution of the system components, such as depletion or enrichment of the grain-boundary region, dominant grain-boundary or bulk precipitation, and also competitive and mixed regimes of formation of secondary phases can be observed in the dependence on the degree of supersaturation, the alloy temperature, and also the character of changes in the interaction parameters near grain boundaries. This model also enables a successful consideration of the formation of precipitate-free zones near grain boundaries. The appearance of complete or partial wetting of the grain boundary can be observed as the interaction parameter near the grain boundaries decreases [17].

The fluctuations are a most substantial factor in the formation of secondary phase precipitates in the region of stable and metastable states, where the overcoming of the nucleation barrier is necessary to form stable nuclei [5]. The fluctuations substantially influence the first-order phase transitions in the systems not containing structural defects [19−23] and also the wetting phase transitions [13]. In this connection, the aim of this work is to generalize the determined model developed before [17, 18] on the case of the existence of thermal fluctuations described within the fluctuation−dissipation theorems [22−26]. In this case, it is necessary to determine the peculiarities of the formation of secondary phase precipitates in the conditions of the fluctuations.

2. MAIN APPROXIMATIONS OF THE MODEL

Consider the formation of the secondary phase precipitates in a three-dimensional cubic fragment of binary alloy with linear size L using the free energy density functional method. Let a plane immobile boundary of two grains described by equation $z = L/2$ be located inside the volume under consideration. According to the assumption of [17], we will believe that the parameter of quasi-chemical interaction Ω is dependent on coordinates $\Omega = \Omega(x, y, z)$ and is described by exponential dependence [18]

$$\Omega(x, y, z) = \Omega_0\left(1 + \Delta\exp\left[-\frac{|z - L/2|}{\delta_0}\right]\right), \qquad (1)$$

where $\Delta = (\Omega_{GB} - \Omega_0)/\Omega_0$ is the parameter the change in that determines the maximum difference between the interaction parameter in bulk (Ω_0) and at the grain boundary (Ω_{GB}). The change in interaction parameter Ω takes place at a small characteristic length δ_0 that is of the order of several lattice parameters ($\delta_0 \ll L$). The sign and the value of parameter Δ influence the character of distribution of the solution components between the grain-boundary region and grain bulk [17, 18]. In this work (for the sake of being definite) we consider the case of a decrease in the parameter of the quasi-chemical interaction when approaching the grain boundary $\Delta < 0$, which corresponds to the effective decrease in the critical temperature and the degree of supersaturation near grain boundaries [17]. The case $\Delta > 0$ in the absence of fluctuations was considered in [18].

The existence of the dependence of the interaction parameter on the concentration field c, and also the effects related to a change in the grain size [27, 28] or the transition of the grain boundary to a liquid state [1] are not considered in this work.

Using the standard methods of the free energy density functional theory [6–8], by analogy with [17, 18], the modified Cahn–Hillard–Cook equation taking into account the dependence of the interaction parameters on coordinates can be obtained

$$\frac{\partial c}{\partial t} = \nabla\left[M\nabla\left(\frac{\partial g}{\partial c} - \nabla(\kappa\nabla c)\right)\right] + \sqrt{\varepsilon}\xi, \qquad (2)$$

where $c \equiv c(x, y, z)$ is the concentration field of the dissolved component, M is the mobility, κ is the gradient energy coefficient that is related to the parameter of quasi-chemical interaction $\kappa = \kappa_0\Omega(x, y, z)a^2$ [17, 18], a is the lattice parameter, κ_0 is the constant depending on the interatomic interaction potential, and ξ is a random Gaussian field, the correlation function of which is described using the fluctuation–dissipation theorem for conserving the order parameter [25, 26]:

$$\langle\xi(\mathbf{r}, t)\xi(\mathbf{r}', t')\rangle = -2Mk_BT\nabla^2\delta(\mathbf{r} - \mathbf{r}')\delta(t - t'), \quad (3)$$

ε is the dimensional quantity that determines the fluctuation amplitude, δ is the Dirac delta function, k_B is

the Boltzmann constant, and $g \equiv g(c)$ is the free mixing energy of alloy per one particle in the regular solution approximation

$$g(c) = \Omega c(1 - c) + k_BT[c\ln c + (1 - c)\ln(1 - c)].$$

For an alloy that has no structural defects, the parameter of quasi-chemical interaction is related to the critical temperature $\Omega = 2k_BT_C$.

In the free energy density functional theory, the displacement of atoms can be characterized by effective diffusion coefficient [7]: $D_{\text{eff}} = M\left.\dfrac{\partial^2 g}{\partial c^2}\right|_{c_M}$. In the considered case ($\Delta < 0$), the ratio of the effective diffusion coefficients at the grain boundary and in grain bulk for the mean composition is $D_{\text{eff}}^b/D_{\text{eff}}^v > 1$, which corresponds to an accelerated diffusion over grain boundaries. This ratio becomes significant ($D_{\text{eff}}^b/D_{\text{eff}}^v \gg 1$) only when approaching the metastability boundary, where the second derivative becomes zero. In addition, a number of alloys demonstrate in practice a substantial (by several orders of magnitude) increase in the diffusion coefficient at grain boundaries (for example, [29–32]) that is likely to be related to a decrease in the diffusion activation energy. The simulation of the evolution of such alloys can be carried out based on the Cahn–Hillard (or Cahn–Hillard–Cook) equation with the inclusion of a variable mobility [33, 34] that should be taken as a quantity depending on coordinates, by analogy with the dependence of the interaction parameter Ω considered in this model [17, 18]. In this work, we do not consider the systems in which the mobility coefficient of the alloy components is changed near grain boundaries.

Going in Eqs. (2), (3) to order parameter $\eta = 2c - 1$ and assuming that mobility M is a constant value, we transform Eq. (2) to form

$$\frac{\partial\eta}{\partial\tau} = \nabla^{*2}[\phi - \nabla^*(\kappa^*\nabla^*\eta)] + \xi^*, \qquad (4)$$

where $\kappa^* = \dfrac{\kappa}{\Omega_0 a^2}$, $\tau = t\dfrac{M\Omega_0}{a^2}$, $\mathbf{r}^* = \mathbf{r}/a$, $\nabla^* = a\nabla$, $\xi^* = \xi\dfrac{2a^2\sqrt{\varepsilon}}{m\Omega_0}$, a is the lattice parameter, and ϕ is the dimensionless function

$$\phi \equiv -2\Omega^*\eta + T^*\ln\left[\frac{1 + \eta}{1 - \eta}\right],$$

where the notations of the dimensionless values are $T^* = 2k_BT/\Omega_0$, $\Omega^* = \Omega(x, y, z)/\Omega_0$. In this case, the random Gaussian field ξ^* corresponds to the correlation function

$$\begin{aligned}\langle\xi^*(\mathbf{r}^*, \tau)\xi^*(\mathbf{r}^*, \tau')\rangle \\ = -4\varepsilon T^*a^{-d}\nabla^{*2}\delta(\mathbf{r}^* - \mathbf{r}^*')\delta(\tau - \tau'),\end{aligned} \qquad (5)$$

where d is the system dimension ($d = 3$).

We believe that the boundary conditions of this alloy fragment are periodic. We will determine the initial condition by a random Gauss distribution of the order parameter that is characterized by a mean value corresponding to alloy composition c_M and a small dispersion of $\sim 10^{-2}$.

3. NUMERICAL METHODS

Taking into account the dependence of the interaction parameters on coordinates [17, 18] and the existence of the fluctuation component [23–26], Eq. (4) can be solved based on the spectral method [33–36] that leads to the difference scheme in the form

$$\hat{\eta}_{\mathbf{k}}^{n+1} = \hat{\eta}_{\mathbf{k}}^{n} + \frac{1}{1 + \Delta\tau\kappa_0\tilde{\Omega}|\mathbf{k}|^4}$$

$$\times (\hat{\xi}_{\mathbf{k}}' - \Delta\tau|\mathbf{k}|^2 \{\hat{\phi}_{\mathbf{k}}^{n} - i\mathbf{k}\mathscr{F}_{\mathbf{k}}[\kappa_0\Omega^*\mathscr{F}_{\mathbf{k}'}^{-1}[i\mathbf{k}'\hat{\eta}_{\mathbf{k}}^{n}]]\}), \qquad (6)$$

where $\hat{\eta}_{\mathbf{k}}^{n}$ is the Fourier transform of the order parameter at the moment of time $\tau_n = n\Delta\tau$, $\mathscr{F}_{\mathbf{k}}[\cdot]$ and $\mathscr{F}_{\mathbf{k}}^{-1}[\cdot]$ are the direct and reciprocal Fourier transforms, respectively, $\hat{\phi}_{\mathbf{k}}^{n}$ is the Fourier transform of the derivative of ϕ on the free energy density at the moment of time τ_n, $\mathbf{k}$ and $\mathbf{k}'$ are wave vectors, $\hat{\xi}_{\mathbf{k}'}'$ is the Fourier transform of the random field $\xi'(\mathbf{r}^*) = \int_{\tau}^{\tau+\Delta\tau} \xi^*(\mathbf{r}^*, \tau')d\tau'$, that is not dependent on time τ with the inclusion of Eq. (5). The dimensional constant $\tilde{\Omega}$ chosen from stability considerations of the difference scheme (6) was taken to be $\tilde{\Omega} = 1$.

From Eq. (5), the expression for the correlation function [20–23] for random values $\xi_{\mathbf{k}}'$ is

$$\langle \hat{\xi}_{\mathbf{k}}' \hat{\xi}_{\mathbf{k}'}' \rangle = \Gamma(\mathbf{k})\delta(\mathbf{k} + \mathbf{k}'),$$

where function $\Gamma(\mathbf{k})$ is determined as

$$\Gamma(\mathbf{k}) = \frac{8\varepsilon\Delta\tau T^*}{Na^d}[3 - \cos(k_x a) - \cos(k_y a) - \cos(k_z a)],$$

where N is the normalization constant of the Fourier transform. Now, the direct calculation of $\hat{\xi}_{\mathbf{k}}'$ can be carried out as $\hat{\xi}_{\mathbf{k}}' = a_{\mathbf{k}} + ib_{\mathbf{k}}$, where $a_{\mathbf{k}}$ and $b_{\mathbf{k}}$ are random quantities that satisfy the Gauss distribution and characterized by a number of properties [19, 20, 23]:

$$\langle a_{\mathbf{k}} \rangle = \langle b_{\mathbf{k}} \rangle = 0, \quad \langle a_{\mathbf{k}}^2 \rangle = \langle b_{\mathbf{k}}^2 \rangle = \frac{1}{2}\Gamma(\mathbf{k}),$$

$$a_{\mathbf{k}} = a_{-\mathbf{k}}, \quad b_{\mathbf{k}} = -b_{-\mathbf{k}}.$$

All alloys have an atomic nature, and this fact should be taken into account by the introduction of the maximum value of wave vector k_{max} (cutoff parameter) [22, 23, 25]. This value implies the absence of the concentration waves of material with the wavelength smaller than $\lambda < 2\pi/k_{max}$. This condition can be reflected using the condition imposed on the Fourier components of a random field ξ': $\xi_{\mathbf{k}}' \equiv 0$ at $|k| > k_{max}$ [20, 25, 36]. The selection of the amplitude and the cutoff parameter (parameters ε and k_{max}) can substantially influence the result of simulating the phase transition process [20–23], including the calculated values of rates of nucleation and the growth of precipitates [23]. This peculiarity is explained by some distortion of the phase equilibrium by fluctuations that can lead to effective change in the critical temperature [37]. Further the simulation will be carried out at the parameters $\varepsilon = 0.25$, $k_{max} = 1.2a^{-1}$ considered in [23].

The secondary phase precipitates were identified using the nearest neighbor method [38] according to the algorithm developed in [34, 39]. The threshold value of the averaged composition that allow us to refer an arbitrary lattice site to the secondary phase was taken to be $C_{min} = 50$ at %. The precipitate size was characterized by equivalent radius R [34, 38]. The precipitate concentration X_C was calculated as $X_C = N_C/V$, where N_C is the total number of observed precipitates, and V is the volume occupied by the system under consideration.

4. SIMULATION RESULTS

The decomposition of the three-dimensional cubic alloy fragment with size $L = 256a$ and having a plane grain boundary with coordinate $z = L/2$ was calculated using the proposed method and the difference scheme (6). The simulation was carried out at temperature $T^* = 0.65$ and alloy compositions $c_M = 10$ and 11 at %. The change in the interaction at the grain boundary was described by values $\Delta = -0.25$, $\delta_0 = 2a$, and $\kappa_0 = 0.2$. The time step was taken to be $\Delta\tau = 5.0 \pm 10^{-4}$.

Figure 1 shows the results of simulation of the evolution of the concentration field. It follows from Fig. 1 that, in the case $c_M = 10$ at %, the regime of the dominant grain-boundary precipitation [17, 18] is observed, which corresponds to a partial wetting of the grain boundary [1, 14–16]. Small nuclei that form far from a grain boundary are unstable and undeniably dissolved, which is most likely related to a high value of the nucleation barrier observed at low degrees of supersaturation [5, 6]. In the case of higher concentration $c_M = 11$ at %, a mixed decomposition regime [17, 18], in which precipitates form both in the grain bulk and at the grain boundary.

In both these cases, the secondary phase precipitates have a lenslike (lamellar) shape at grain boundaries and a shape close to spherical ingrain bulk. The observed geometry of precipitates (Fig. 1) at the grain boundary and in the grain volume with the results of experimental studies of the wetting phase transitions at grain boundaries for a number of alloys [14–16].
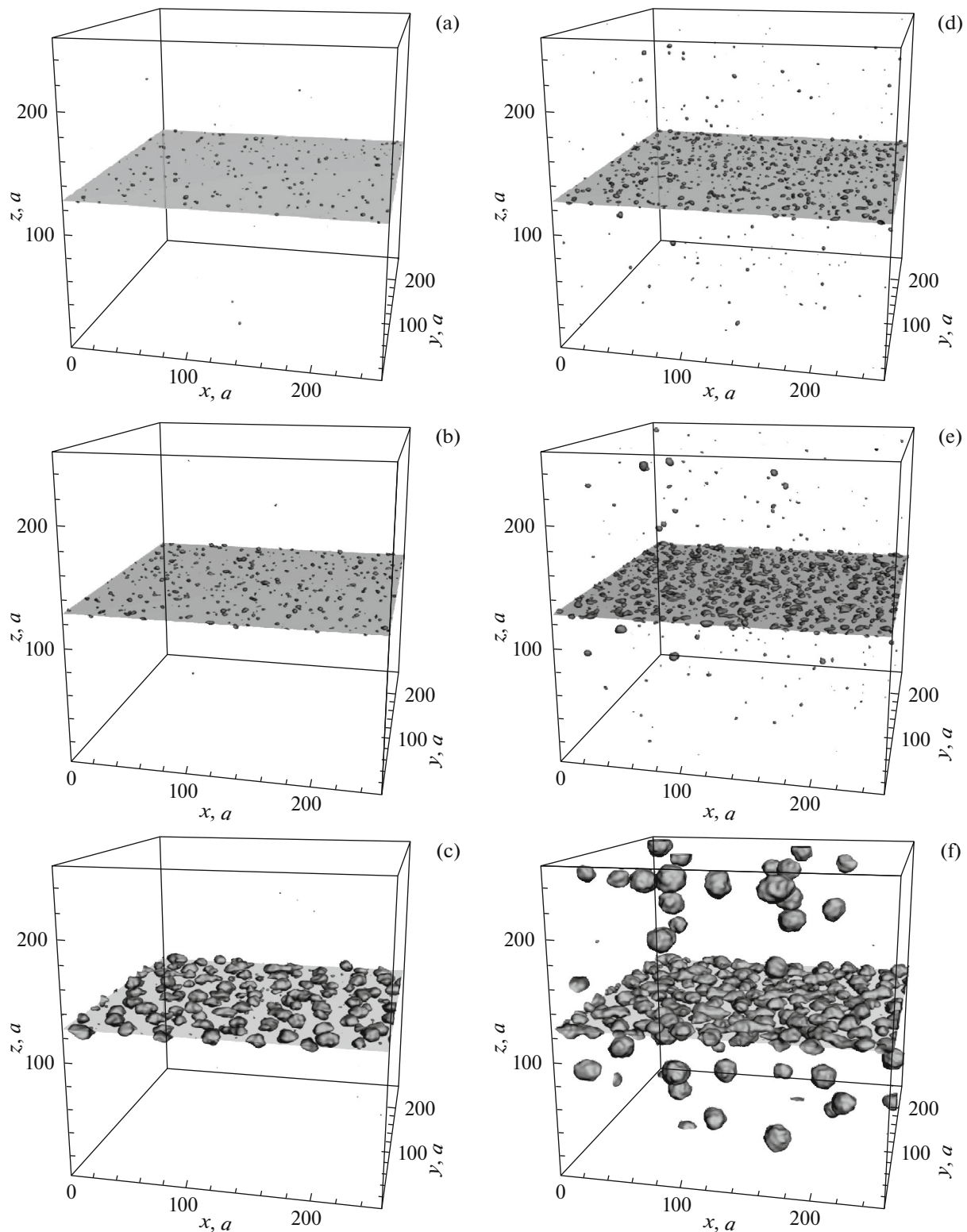
Fig. 1. Phase distribution in binary alloys with compositions (a, b, c) $c_M = 10$ at % and (d, e, f) $c_M = 11$ at % at temperature $T^* = 0.65$ and at different moments of time: (a, d) $\tau = 75$, (b, e) $\tau = 150$, (c, f) $\tau = 900$.

The existence in the system of long-wavelength fluctuations lead to the appearance of a surface relief of precipitates disposed in the grain bulk [23] and at the grain boundaries, too. The fluctuations also cause the inconstancy of the contact angle that can be changed during grain growth within quite wide limits.
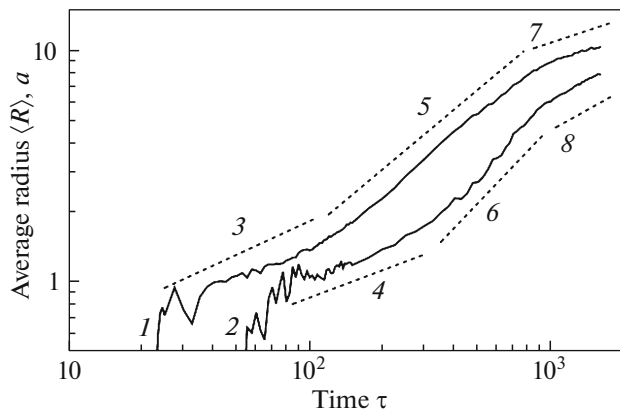
Fig. 2. Dependence of precipitate mean size $\langle R \rangle$ in binary alloy on annealing time τ for alloys (curve *1*) $c_M = 11$ at % and (curve *2*) $c_M = 10$ at %. The dotted lines show the approximation of corresponding calculation data by the power functions $\langle R \rangle \propto \tau^\alpha$: $\alpha = $ (*3*) 0.48 ± 0.02, (*4*) 0.39 ± 0.03, (*5*) 0.87 ± 0.01, (*6*) 1.1 ± 0.03, (*7*) 0.34 ± 0.01, and (*8*) 0.59 ± 0.01.

Fig. 3. Dependence of precipitate concentration X_C on annealing time τ for the alloys with compositions (curve *1*) $c_M = 11$ at % and (curve *2*) $c_M = 10$ at % at temperature $T^* = 0.65$.

When analyzing the contact angles of coarse precipitates that form at grain boundaries of the considered alloys at the late stage, the angles were $52° \pm 10°$ for $c_M = 11$ at % and $56° \pm 11°$ for $c_M = 10$ at %. The coincidence of the obtained contact angles within the limits of the error is quite expected and is provided at the same temperatures and interaction parameters for both alloys.

To study the kinetics of the mean size, the concentration, the distribution function of precipitates at the initial stage ($\tau < 275$), the independent simulations were carried out for four solid solution fragments using the difference scheme (6). The characteristics of the phase distribution for this interval were determined by their averaging over all independent realizations [18, 40]. For later time intervals ($\tau > 275$), one attempt of the calculations was carried out because of substantial calculation time. In the range $0 < \tau < 1600$, the calculation duration was about four days.

Figures 2 and 3 show the calculation results of the kinetics of the precipitate mean size and their concentration, respectively. As follows from Figs. 2 and 3, the known mechanisms of formation of the secondary phase precipitates (nucleation, growth, coagulation, and coalescence) are observed in the compositions and for time intervals considered in this work. In addition, the growth rate of the precipitate mean size is substantially different from the known dependences established in the classical nucleation theory [5, 41] for the stages of diffusion growth ($\langle R \rangle \sim \tau^{1/2}$) and coalescence ($\langle R \rangle \sim \tau^{1/3}$). These dependences are quite well confirmed based on the simulation of nucleation in binary alloys with a constant mobility that does not contain structural defects in the absence of the composition fluctuations [34, 42].
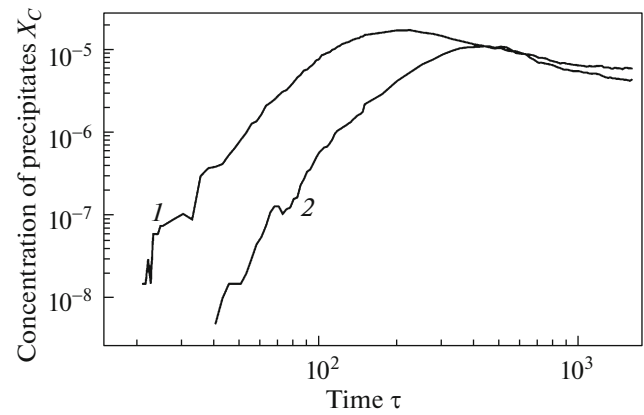
At the stage of nucleation, the mean size growth close to a power law was observed in both considered cases. In this case, the stage of diffusion growth was characterized by an accelerated growth of the precipitate mean size as compared to the classical theory of diffusion growth, according to which the precipitate radius must be changed as $R \sim \tau^{1/2}$ [5, 41]. The reason of the anomalous power growth at the initial stage is a combination of decomposition mechanisms observed at considered low concentrations of the dissolved component. So, at the initial stage, the nuclei form during fairly long time. The stable nuclei formed earlier undergo the diffusion growth due to the inflow of atoms from the matrix. Simultaneously, new nuclei form; in this case, the effective mean size growth rate is lower than that assumed by the diffusion growth theory $\langle R \rangle \sim \tau^\alpha$ ($\alpha < 1/2$). Then, as the degree of supersaturation decreases, the nuclei formed later are in an unstable state and are dissolved fast. This process is combined with continuing diffusion growth of stable nuclei, which leads to the effective growth of the mean size $\langle R \rangle \sim \tau^\alpha$ ($\alpha > 1/2$). The existence of the grain boundaries also provides different rates of formation and growth of the precipitates in the bulk and at the grain boundaries, that are actually at different stages of decomposition, which exactly leads to a change in the exponent α.

The growth rate is substantially slowed down to the end of the time interval under consideration ($\tau > 1000$), and this fact can be due to a gradual transition to the coalescence stage. This intermediate stage (also [34, 40, 42]) is characterized by a slight increase in the mean size as the precipitate concentration decreases slowly. The intermediate stage is expected can be substantially longer than that for the alloy without grain boundaries [34, 42], which is related to a combination of several mechanisms: coagulation (coalescence) of precipitates located at a grain boundary and also the
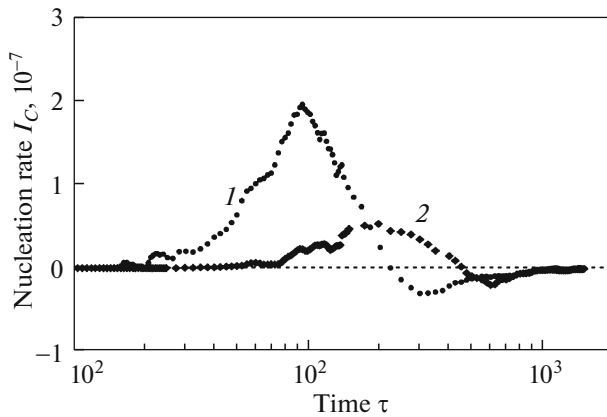
Fig. 4. Dependence of nucleation rate I_C of the secondary phase precipitates in the binary alloys characterized by compositions (curve *2*) $c_M = 10$ at % and (curve *1*) $c_M = 11$ at % at temperature $T^* = 0.65$.

diffusion growth of these precipitates due to a material coming from the matrix. At this stage, we also observe the dissolution of fine precipitates characteristic of the coalescence mechanism; however, this mechanism is not dominant. In addition, the fluctuations also substantially influence the processes of material transfer and the growth of precipitates (also, [23]). The study of the growth of the secondary phase precipitates at the later stage requires the increase in computer power or the simulation time approximately by one–two orders and also substantial increase in the system size.

This model can be also used to state some peculiarities of the kinetics of the formation of the second phase precipitates. The precipitate growth rate can be determined as the derivative on the concentration of observed precipitates $I_C = dX_C/d\tau$ [43]. In the classical and nonclassical nucleation theories, this quantity is usually associated with supercritical nuclei [5, 41, 43]. In this case, the interaction parameters are dependent on coordinates and the change in the alloy composition over the system volume at the nucleation stage is determined by the fluctuations. In this case, it seems to be impossible to distinguish the supercritical nuclei from other nuclei and inhomogeneities of the composition formed in the system due to the fluctuations [23, 34, 43]. In this connection, the quantity I_C is actually a detectable nucleation rate [43], the value of which can be dependent on the used method of identification of the nuclei.

Figure 4 shows the dependence of the nucleation rate for two considered alloy compositions. Since the considered quantity has a substantial random component, when constructing these curves, the smoothing by the moving average method was used [44]. As follows from Fig. 4, the decrease in the alloy composition leads to a decrease in the nucleation rate and also to a marked increase in the incubation time of nucleation.

This feature agrees well with the conclusions of the nonclassical nucleation theory [5, 6], in which it was stated that the critical size and the incubation time increases as the degree of supersaturation (for example, [34, 45, 46]).

The considered approach that also allows one to observe the evolution of the size distribution function, the results of calculation of which for the considered alloys ($c_M = 10$ and 11 at %) are shown in Fig. 5. As follows from these plots, the distribution functions for the considered alloys demonstrate the evolution similar to that of the alloys that have not structural defects [23, 34, 42]. At initial stage, nucleus sizes have a quite wide scatter: the maximum value of R can be larger by a factor of more than two ($u_{max} > 2.0$) than $\langle R \rangle$ (Figs. 5a and 5c). At the later stage, the distribution function approaches a function that is determined by the Lifshitz–Slyozov theory ($u_{max} \sim 3/2$). The formation of the stationary size distribution function for the alloy with a lower composition slows down noticeably (Figs. 5b, 5c). It should be noted that, at the later stage, the shape of the stationary size distribution function is substantially dependent on the mechanism of material transfer [47]. In general case, the combination of several mechanisms or the dominance of one of them (for example, the grain-boundary diffusion) can lead to the distribution functions that substantially distinguish from the conclusions of the Lifshitz–Slyozov theory built for the case of the volume diffusion of the dissolved component [47]. In the systems that are characterized by various mass-transfer mechanisms, we expect the appearance of stationary distribution functions of the precipitates with various values of parameter u_{max}. Despite the substantially different conditions of formation of the precipitates, we did not observe principal differences between the distribution functions for the cases of the grain-boundary precipitation ($c_M = 10$ at %) and a combined decomposition regime ($c_M = 11$ at %) considered in this work, and this fact is likely to be related to the dominance of the material transfer over the system volume. A possible reason of insignificant difference of the distribution function is also an insufficiency of the time interval during which the stationary distribution function could not be attained.

5. CONCLUSIONS

Based on the model developed and the simulation carried out in this work, we can make the following conclusions on the process of precipitation at grain boundaries that can be observed if the introduction parameter between the solution components decreases when approaching the grain boundary.

The most pronounced influence of grain boundaries on the precipitation is observed at low degrees of supersaturation. In this case, the formation of nuclei occurs immediately at the grain boundary, and no pre-
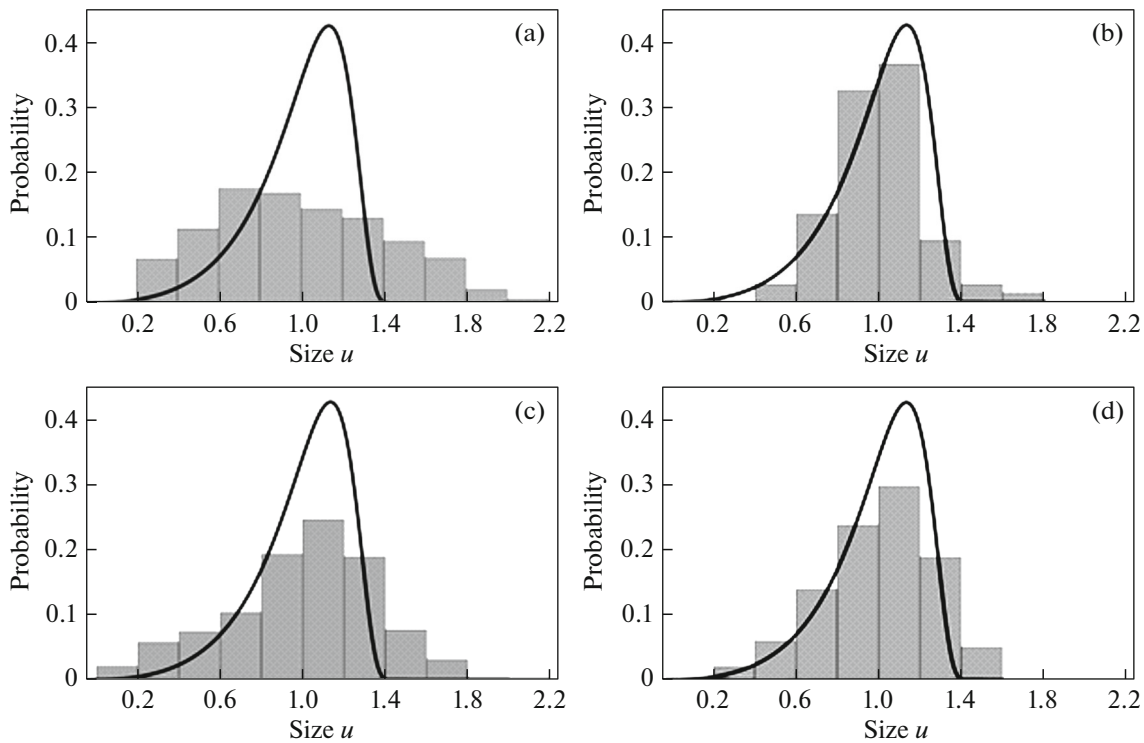
Fig. 5. Size distribution function ($u = R/\langle R \rangle$) in the case of precipitate formation at grain boundaries for the alloys with compositions (a, b) $c_M = 10$ at % and (c, d) $c_M = 11$ at % at different moments of time $\tau = $ (a, c) 400 and (b, d) 1600 at temperature $T^* = 0.65$. The solid line shows the size distribution function according to the Lifshitz–Slyozov theory.

cipitates are observed in the grain bulk. The main reason is a decrease in the nucleation barrier near grain boundaries due to a lower interaction parameter. The overcoming of the nucleation barrier is provided due to long-wavelength fluctuation of the alloy composition.

An increase in the dissolved component concentration leads to the transition to a combined mechanism of formation of the precipitates when stable nuclei form both in the grain bulk and at the grain boundaries and also to an increase in the fluctuation nucleation rate and a decrease in the incubation time. In this case, the durations of the nucleation and diffusion growth stages decrease.

The fluctuations lead to the appearance of surface relief of the precipitates, which substantially influences the determined contact angles. The contact angle can be changed within fairly wide limits as the precipitates grow, but it is changed less substantially for coarse precipitates formed at the later stage.

The fluctuations and the dependence of the interaction parameters on coordinates related to the existence of the grain boundaries lead to the appearance of some features of the precipitate growth. At the initial stage, we can separate a portion of a weak power growth of precipitates ($\langle R \rangle \propto \tau^\alpha$, $\alpha \sim 0.3$). At the stage of diffusion growth, the existence of grain boundaries

and composition fluctuations can lead to the appearance of accelerated growth of precipitates ($\alpha > 1/2$). In the case of the dominant grain-boundary precipitation, the transition to the coalescence stage can be retarded substantially. The accelerated growth can be caused by a complex of causes related to the system under consideration. First, the existence of the composition fluctuations leads to simultaneous observation of several mechanisms of the secondary phase formation: the nucleation, the diffusion growth, and the dissolution of precipitates, and also their coalescence (coagulation). This combination of various mechanisms of the secondary phase formation can substantially influence the growth rate of the mean size of the secondary phase precipitates. Second, a decrease in the interaction energy near the grain boundary leads to the difference of the degrees of supersaturations in the grain bulk and at the grain boundaries; in this case, the effective diffusion coefficient near grain boundaries increases, which causes the difference of material flows along the grain boundary and from the grain bulk to the boundary. In addition, since the secondary phase formation and the growth rates at the grain boundaries and in the grain bulk are different, the grain decomposition in these regions can be at different stages, which also causes a change in the growth rate of the precipitate size and

the concentration averaged over the entire system under consideration.

ACKNOWLEDGMENTS

REFERENCES

1. B. B. Straumal, *Grain Boundary Phase Transitions* (Nauka, Moscow, 2003) [in Russian].

2. *Physical Metallurgy*, Ed. by R. W. Cahn and P. Haasen (North-Holland, Amsterdam, 1996; Metallurgiya, Moscow, 1987).

3. L. Priester, *Grain Boundaries: From Theory to Engineering* (Springer, Dordrecht, 2013).

4. P. Lejček, M. Všianská, and M. Šob, J. Mater. Res. **33**, 2647 (2018).

5. K. Kelton and A. Greer, *Nucleation in Condensed Matter* (Elsevier, Amsterdam, 2010).

6. J. W. Cahn and J. E. Hilliard, J. Chem. Phys. **31**, 688 (1959).

7. J. Cahn, Acta Metall. **9**, 795 (1961).

8. N. Provatas and K. Elder, *Phase-Field Methods in Material Science and Engineering* (Wiley-WCH, Weinheim, 2010).

9. J. Cahn, J. Chem. Phys. **66**, 3667 (1977).

10. D. Bonn, J. Eggers, J. Indekeu, J. Meunier, and E. Rolley, Rev. Mod. Phys. **81**, 739 (2009).

11. A. A. Pahlavan, L. Cueto-Felgueroso, A. E. Hosoi, G. H. McKinley, and R. Juanes, J. Fluid Mech. **845**, 642 (2018).

12. K. Mahdy, A. Afkhami, and L. Kondic, Phys. Fluids **26**, 62002 (2016).

13. G. Grün, K. Mecke, and M. Rauscher, J. Stat. Phys. **122**, 1261 (2006).

14. O. A. Kogtenkova, A. B. Straumal, N. S. Afonikova, A. A. Mazilkin, K. I. Kolesnikova, and B. B. Straumal, Phys. Solid State **58**, 742 (2016).

15. A. S. Gornakova, B. B. Straumal, A. N. Nekrasov, A. Kilmametov, and N. S. Afonikova, J. Mater. Eng. Perform. (2018). doi 10.1007/s11665-018-3300-3

16. B. B. Straumal, O. A. Kogtenkova, M. Yu. Murashkin, M. F. Bulatov, T. Czeppe, and P. Zięba, Mater. Lett. **186**, 82 (2017).

17. P. E. L'vov and V. V. Svetukhin, Phys. Solid State **59**, 2453 (2017).

18. P. E. L'vov and V. V. Svetukhin, Phys. Solid State **60**, 791 (2018).

19. J. Fan, M. Sammalkorpi, and M. Haataja, Phys. Rev. E **81**, 11908 (2010).

20. T. M. Rogers, K. R. Elder, and R. C. Desai, Phys. Rev. B **37**, 9638 (1988).

21. K. R. Elder, T. M. Rogers, and R. C. Desai, Phys. Rev. B **38**, 4725 (1988).

22. J. García-Ojalvo and J. M. Sancho, *Noise in Spatially Extended Systems* (Springer, New York, 1999).

23. P. E. L'vov and V. V. Svetukhin, Mod. Simul. Mater. Sci. Eng. **26**, 045001 (2018).

24. H. Cook, Acta Mater. **18**, 297 (1970).

25. P. C. Hohenberg and B. I. Halperin, Rev. Mod. Phys. **49**, 435 (1977).

26. X. Li, G. Ji, and H. Zhang, J. Comp. Phys. **283**, 81 (2015).

27. V. B. Fedoseev, Phys. Solid State **57**, 599 (2015).

28. V. B. Fedoseev and E. N. Fedoseeva, JETP Lett. **97**, 408 (2013).

29. J. C. Fisher, J. Appl. Phys. **22**, 74 (1951).

30. Y. Mishin, Chr. Herzig, J. Bernardini, and W. Gust, Int. Mater. Rev. **42**, 155 (1997).

31. V. V. Popov, A. V. Sergeev, N. K. Arkhipova, and A. Yu. Istomina, Phys. Met. Metallogr. **112**, 256 (2011).

32. R. T. Sibatov and V. V. Svetukhin, Phys. Lett. A **381**, 2021 (2017).

33. J. Zhu, L.-Q. Chen, J. Shen, and V. Takare, Phys. Rev. E **60**, 3564 (1999).

34. P. E. L'vov and V. V. Svetukhin, Mod. Simul. Mater. Sci. Eng. **25**, 075006 (2017).

35. L.-Q. Chen and J. Shen, Comput. Phys. Commun. **108**, 147 (1998).

36. S. Muralidharan, R. Khodadad, E. Sullivan, and M. Haataja, Phys. Rev. B **85**, 245428 (2012).

37. L. D. Landau and E. M. Lifshitz, *Course of Theoretical Physics*, Vol. 5: *Statistical Physics* (Nauka, Moscow, 1976; Pergamon, Oxford, 1980).

38. M. Miller and R. Forbes, *Atom-Probe Tomography: The Local Electrode Atom Probe* (Springer, New York, 2014).

39. P. E. L'vov and V. V. Svetukhin, State Registration Certificate of Computer Program No. 2017616554 (2017).

40. P. E. L'vov and V. V. Svetukhin, Phys. Solid State **58**, 1432 (2016).

41. H. Aaronson, M. Enomoto, and J. Lee, *Mechanisms of Diffusional Phase Transformations in Metals and Alloys* (CRC, Taylor and Francis Group, Boca Raton, FL, 2010).

42. P. E. L'vov and V. V. Svetukhin, Phys. Solid State **59**, 355 (2017).

43. D. Kashchiev, *Nucleation. Basic Theory with Applications* (Butterworth-Heinemann, Eastbourne, 2000).

44. G. S. Kil'dishev and A. A. Frenkel, *Time Series Analysis and Forecasting* (Statistika, Moscow, 1973) [in Russian].

45. F. K. LeGoues and H. I. Aaronson, Acta Met. **32**, 1855 (1984).

46. B. Li, L. Zhang, C. Li, Q. Li, J. Chen, G. Shu, Y. Weng, B. Xu, and W. Liu, Mod. Simul. Mater. Sci. Eng. **25**, 085006 (2017).

47. V. V. Slezov and V. V. Sagalovich, Usp. Fiz. Nauk **151**, 67 (1987).

Translated by Yu. Ryzhkov